Acta Mechanica Sinica (2020) 36:1294–1301
https://doi.org/10.1007/s10409-020-00982-z

RESEARCH PAPER

Similarities in the penetration depth of concrete impacted by rigid projectiles

C. G. Chai[1] · **A. G. Pi**[2] · **Q. M. Li**[3] · **F. L. Huang**[2]

Received: 15 March 2020 / Revised: 26 May 2020 / Accepted: 27 July 2020 / Published online: 20 October 2020

Abstract

Similarity can reflect common laws in the mechanism of rigid-body penetration. In this paper, the similarities in rigid-body penetration depth are demonstrated by three non-dimensional but physically meaningful quantities, i.e., ρ_{kinetic}, I^*_{ln} and N'_1. These three quantities represent the non-dimensional areal density of projectile kinetic energy, the effect of nose geometry, and the friction at the interactive cross section between projectile and target respectively. It is shown that experimental data of rigid projectile penetration, from shallow to deep penetration, can be uniquely unified by these three similarity quantities and their relationships. Furthermore, for ogival nose projectiles, their penetration capacities are dominated by ρ_{kinetic}, which is consisted by non-dimensional effective length L_{eff} and non-dimensional quantity $D^{\text{p}}_{\text{n}} = \frac{\rho_{\text{p}} v_0^2}{AY}$ which has the same form as Johnson's damage number. On the sacrifice of minor theoretical accuracy, the non-dimensional penetration depth P/d can be understood as directly controlled by D^{p}_{n}, enhanced by projectile effective length L_{eff} under a multiplication relation, and optimized by projectile nose geometry in the formation of I^*_{ln}.

Keywords Concrete target · Deep penetration · Similarity · Johnson's damage number

1 Introduction

Penetration into reinforced and plain concrete targets by hard projectiles has been investigated extensively for both civil and military applications [1–5]. Considering the high cost of penetration experiments, especially for large scale and high velocity impact experiments, it is necessary to investigate the relations between the laboratory-based small scale experiments and large scale prototype experiments, i.e., the similarity and scaling laws for the penetration of concrete target. Peng et al. [6] discussed whether the scaling law holds or not for small-scale experiments to large-scale penetration scenarios and found that the scaling law satisfies for depth prediction of penetration in rigid projectile penetration as long as the scaling is done strictly for both projectiles and concrete targets including the coarse aggregates. However, the scaling effect of penetration and the applicable condition of homogeneous assumption of concrete inhibit a further understanding of the scaling in concrete penetration. Wu et al. [7, 8] evaluated the existing empirical formulae, theoretical model and penetration tests and attributed the scaling effect mainly to the inconsistent variations of projectile diameter and coarse aggregates size in the scaled impact tests. Zhang et al. [9, 10] investigated the properties of coarse aggregates and reinforcement on penetration resistance using 3D meso-scale modelling and cavity-expansion model, and proposed the applicable condition of the homogeneous assumption of concrete that the sensitivity of penetration resistance to aggregate size is lower than other mesoscopic factors like mortar strength, aggregate strength and volume fraction.

The similarity in concrete penetration has already been discussed using dimensional analysis by introducing two non-dimensional numbers, i.e., the impact function (I) and geometry function of projectile (N) [3], which are expressed as

✉ A. G. Pi
aiguo_pi@bit.edu.cn

C. G. Chai
chaicg@caep.cn

1 Institute of Chemical Materials, China Academy of Engineering Physics, Mianyang 621900, China

2 State Key Laboratory of Explosion Science and Technology, Beijing Institute of Technology, Beijing 100081, China

3 School of Mechanical, Aerospace and Civil Engineering, University of Manchester, Manchester M13 9PL, UK

$$I = \frac{Mv_0^2}{N_1' d^3 Y} \bigg/ A, \tag{1}$$

$$N = \frac{M}{\rho_t d^3} \bigg/ N^*, \tag{2}$$

where M, v_0, and d are the mass, initial impact velocity, and diameter of projectile, respectively; ρ_t and Y are concrete target density and uniaxial compressive strength; N_1' and N^* are coefficients related to friction and projectile nose geometry respectively, expressed as Eqs. (5) and (7); A is a constant related to target dynamic resistance. However, the understanding and influences of these two non-dimensional numbers were only carried out as collective quantities, without discussion on the influencing mechanism of their constituent parameters.

In this paper, further derived from the afore two widely accepted non-dimensional numbers [3], three integrated non-dimensional quantities, i.e., ρ_{kinetic}, $I^*_{\ln}$ and N_1', are proposed to provide a better understanding on the similarities in rigid-body penetration. The effects and physical meanings of each of these three non-dimensional quantities are discussed based on experimental data and analytical equations including the friction at the interactive cross section between target and projectile surfaces. The similarities and their parameters for the penetration depth of rigid ogival nose projectiles are discussed based on the similarity relationships.

2 Non-dimensional quantities influencing penetration depth

Neglecting crater regime in the initial impact stage, which is valid for deep penetration, the normal penetration resistance and non-dimensional penetration depth considering the friction on the shank of an ogival nose projectile shown in Fig. 1 can be expressed as [11]

$$F_x = \frac{\pi d^2}{4}\left(N_1' AY + N_2 B \rho_t v^2\right), \tag{3}$$

$$\frac{P}{d} = \frac{2M}{N_2 B \rho_t \pi d^3} \ln\left(1 + \frac{N_2 B \rho_t v_0^2}{N_1' AY}\right), \tag{4}$$

where

$$N_1' = 1 + 4\mu\psi^2\left[\left(\frac{\pi}{2} - \phi_0\right) - \frac{\sin(2\phi_0)}{2}\right] + \frac{4\mu(L_0 - h)}{d}, \tag{5}$$

$$N_2 = N^* + \mu\psi^2\left\{\left(\frac{\pi}{2} - \phi_0\right) - \frac{1}{3}\left[2\sin(2\phi_0) + \frac{\sin(4\phi_0)}{4}\right]\right\}, \tag{6}$$

$$N^* = \frac{1}{3\psi} - \frac{1}{24\psi^2}, \tag{7}$$

$$\phi_0 = \sin^{-1}\left(1 - \frac{1}{2\psi}\right), \tag{8}$$

where v is the penetrating velocity and caliber-radius-head (CRH) $\psi = s/d$ and μ is the coefficient of friction. For concrete, B varies in a small range, and is commonly taken as 1.0 [3, 12].

Taking

$$I^* = \frac{N_2}{N_1'} \frac{\rho_t v_0^2}{AY}, \tag{9}$$

$$I_0 = \frac{Mv_0^2}{d^3 AY} = \frac{\pi}{4} \frac{\rho_p v_0^2}{AY} \frac{L_{\mathrm{eff}}}{d}, \tag{10}$$

where projectile effective length L_{eff} is defined by $M = \rho_p \pi d^2 L_{\mathrm{eff}}/4$. L_{eff} was proposed to replace the old nominal projectile length L_0 to account the influences of inner hollow structures of projectile [13]. Then, Eq. (4) can be rewritten as

$$\frac{P}{d} = \frac{1}{N_1'} \frac{2}{\pi} I_0 \frac{\ln(1 + I^*)}{I^*} = \rho_{\mathrm{kinetic}} I^*_{\ln} / N_1', \tag{11}$$

where

$$\rho_{\mathrm{kinetic}} = \frac{\frac{1}{2}\rho_p v_0^2}{AY} \frac{L_{\mathrm{eff}}}{d} = \frac{1}{2} D_n^p \frac{L_{\mathrm{eff}}}{d}, \tag{12}$$

$$I^*_{\ln} = \frac{\ln(1 + I^*)}{I^*}. \tag{13}$$

Based on Eqs. (4–11), it can be seen that influential factors can be integrated into the combination of three

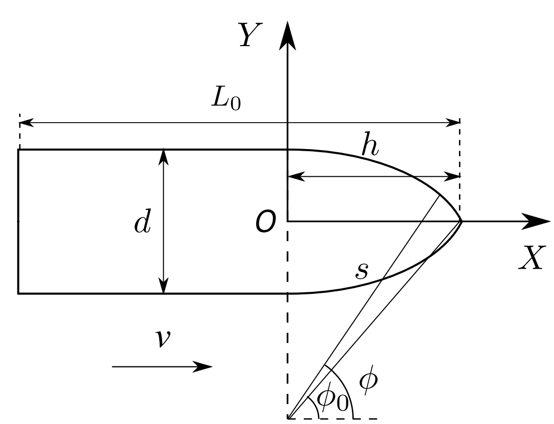

Fig. 1 Schematic diagram of a projectile

non-dimensional quantities, i.e., ρ_{kinetic}, the non-dimensional areal density of projectile kinetic energy (KE) relative to non-inertia resistant stress of target at the interactive cross section between projectile and target; I^{*}_{ln}, combined factor of projectile nose geometry (N_2), friction imposed on projectile (N'_1), and non-dimensional number ($D^{\text{t}}_{\text{n}} = \frac{\rho_{\text{t}} v_0^2}{AY} = \frac{\rho_{\text{t}}}{\rho_{\text{p}}} D^{\text{p}}_{\text{n}}$); and N'_1, coefficient related to the friction.

2.1 ρ_{kinetic}, the non-dimensional areal density of projectile KE relative to non-inertia resistant stress of target

Non-dimensional number, $\rho_{\text{kinetic}} = \frac{1}{2} \frac{\rho_{\text{p}} v_0^2}{AY} \frac{L_{\text{eff}}}{d}$, is the non-dimensional areal density of projectile KE relative to non-inertia resistant stress of target. Quantity ρ_{kinetic} consists of two non-dimensional quantities, i.e., areal density of kinetic energy per unit effective length of the projectile, $(\rho_{\text{p}} v_0^2 / 2)/(AY)$, and ratio of the effective projectile length to projectile diameter, L_{eff}/d, as seen in Eq. (12). They together define ρ_{kinetic} as the ratio between initial projectile KE and non-inertia resistance of target, which is already normalized by the projectile cross-sectional area.

ρ_{kinetic} dominates the penetration capability of a projectile, and the non-dimensional penetration depth P/d increases almost linearly with the increase of ρ_{kinetic}, as shown in Fig. 2. For given target and projectile with certain initial velocity, $(\rho_{\text{p}} v_0^2 / 2)/(AY)$ becomes constant, as a result, the non-dimensional penetration depth P/d would approximately increase according to non-dimensional effective length L_{eff}/d, instead of non-dimensional nominal length L_0/d. For given projectile with fixed L_{eff}/d, the non-dimensional penetration depth P/d would approximately increase according to $((\rho_{\text{p}} v_0^2 / 2)/(AY)$. This approximate linear relationship supports the conclusion that the penetration resistance of concrete is constant [13]. However, it is contradictory with the fact that penetration resistance increases with the increase of impact velocity, where the average resistance (defined as $\frac{1}{2} M v_0^2 / P$) of high impact velocity is higher than that of low velocity [19]. In fact, this linear relationship or constant resistance only works when resistance proportion of both I^{*}_{ln} and N'_1, which represent the combined effects of projectile nose geometry, D^{t}_{n}, and friction, are surprisingly limited, e.g., in the experimented velocity range shown in Fig. 2. In this velocity range, to the most, the combined resistance proportion only accounts for less than 20% [11]).

The afore linear relationship applies only to certain scopes. This scopes consists of two aspects: the penetration velocity and projectile nose geometry. To the penetration velocity, this linear relationship only applies when the penetration velocity would not cause severe projectile erosion where rigid-body penetration assumption applies. Furthermore, this velocity should not be too low where only a crater region forms. For the crater region, the rapid resistance change during the crater process introduces a nonlinear resistance relationship, in other words, this linear relationship doesn't apply when crater region dominates. However, through the application of non-dimensional parameter ρ_{kinetic}, this nonlinear relationship still shows similarity between scaled projectiles but not as a linear relations as shown later. To the projectile nose, surprisingly all the projectiles with arc nose geometries can be unified through the similar number I^{*}_{ln} if the afore conditions are satisfied.

2.1.1 Effects of constituent parameters of Johnson's damage number

Non-dimensional quantity $D^{\text{p}}_{\text{n}} = \rho_{\text{p}} v_0^2/(AY)$ has the same form as Johnson's damage number defined as $D_{\text{n}} = \rho v^2 / \bar{Y}$, about which further clarifications are needed. As realized by Johnson [20] that "Some weaknesses attaching to the use of this damage number are (i) that no account is taken of projectile nose shapes, (ii) it is not clear what meaning or value is to be given to $\bar{Y}$ when the damage number is large, …". The effects of projectile nose shapes will be explained by I^{*}_{ln} later in Sect. 2.2. $\bar{Y}$ can be interpreted as the dynamic strength resistance of the target (AY).

This assumption is supported by the linear relationship between $P/\left(L_{\text{eff}} I^{*}_{\text{ln}}\right)$ and $D^{\text{p}}_{\text{n}} = \frac{\rho_{\text{p}} v_0^2}{AY}$, shown in Fig. 3, where $P/\left(L_{\text{eff}} I^{*}_{\text{ln}}\right)$ is the normarlized P by excluding the effects of effective length L_{eff} and projectile nose geometry I^{*}_{ln}, and the friction effect is included intentionally to further support the conclusion that the friction affects limitedly and can be taken as a constant for engineering accuracy [11]. Comparing with the approximately linear relationship between $\frac{P}{d}$ and $\rho_{\text{kinetic}} = \frac{\frac{1}{2} \rho_{\text{p}} v_0^2}{AY} \frac{L_{\text{eff}}}{d}$ shown in Fig. 2, it can be seen in Fig. 3 that after excluding the effects of projectile nose geometry (represented by I^{*}_{ln}) and L_{eff}, the normalized penetration depth P is still linear with D^{p}_{n}, which means that penetration depth P/d is both linear with D^{p}_{n} and L_{eff}, respectively. Hence, it

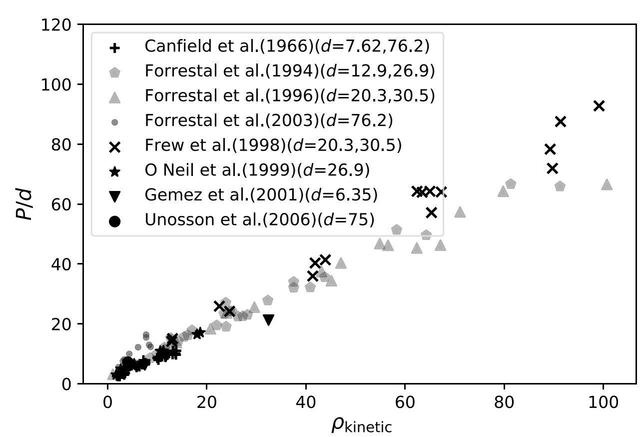

Fig. 2 Relationship between P/d and ρ_{kinetic} [1, 2, 12, 14–18]

can be concluded that P/d is directly linearly controlled by D_n^p, enhanced by L_{eff}/d under the multiplication relation, and optimized by projectile nose geometry in the formation of I_{ln}^*. Furthermore, after excluding the influences of projectile nose geometry and friction, it can be concluded that D_n^p can be understood as the non-dimensional initial intensity of impact or the order of strain imposed at the interactive cross section between projectile and target where severe plastic deformation occurs, while L_{eff}/d represents the non-dimensional duration of this D_n^p, or they together represent the non-dimensional total kinetic energy of the projectile. For the same D_n^p with a given nose geometry, the larger the L_{eff}/d is, the deeper the projectile can penetrate.

2.2 I_{ln}^*, combined effect factor of nose geometry and D_n^t

From the definition of I_{ln}^* in Eqs. (9) and (13), I_{ln}^* is a function in terms of projectile nose geometry (N_2), friction imposed on projectile (N_1'), and non-dimensional number (D_n^t). I_{ln}^* is apparently dependent on $\rho_{kinetic}$ and N_1', these three similarity numbers are not independent with each other. However, the dependency of I_{ln}^* on other two numbers can be approximately eliminated conditionally and I_{ln}^* would be left as the only function of projectile nose geometry (N_2). The improved more obvious linear trend shown in Fig. 3 (representing the approximately linear relationship between $P/(L_{eff}I_{ln}^*)$ and D_n^p) than Fig. 2 (representing the approximately linear relationship between P/d and $\rho_{kinetic} = \frac{1}{2}D_n^pL_{eff}/d$) demonstrates that certain mechanism has been represented correctly, where the only difference is that in Fig. 3 the effect of I_{ln}^* was included. The dependency of I_{ln}^* on $\rho_{kinetic}$ is by $D_n^p = \frac{\rho_p}{\rho_t}D_n^t$ and its own D_n^t. However, when the target properties and projectile initial velocity are fixed, D_n^t and D_n^p would be correlated into one, i.e., $D_n^p = \frac{\rho_p}{\rho_t}D_n^t$, in other words, when D_n^p is fixed at the impact

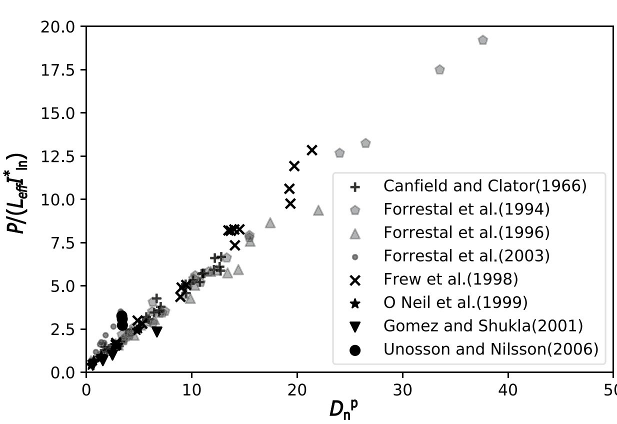

Fig. 3 Relationship between $P/(L_{eff}I_{ln}^*)$ and D_n^p [1, 2, 12, 14–18]

beginning, D_n^t would also be fixed as a constant as a consequence. Furthermore, $\rho_{kinetic}$ is the dominant parameter and the effects of I_{ln}^* in penetration depth is very limited for concerned ogival nose projectiles compared with $\rho_{kinetic}$. In addition, it has been justified that for the majority of experimented projectiles, friction resistance only accounts for around 10% in total penetration resistance, which means that N_1' can be taken as constant 1.09 [11]. Hence, I_{ln}^* would be left only as the effects of projectile nose geometry. In other words, when target properties and projectile initial velocity are fixed, I_{ln}^* is the only function of nose geometry N_2 and N_1', and for projectiles with the same or scaled geometries, N_1' would be the same, then I_{ln}^* would be left as the only function of nose geometry N_2. This idealized assumption can be further supported by Fig. 4 in which the effect of L_{eff} has been normalized in the normalization process of P/L_{eff}, as a result, Fig. 4 is showing the relationships between normalized penetration depth and its dependency on nose geometry (N_2).

The relationship between P/L_{eff} and I_{ln}^* is shown in Fig. 4. It is shown that even though all the experimented projectiles are different remarkably in their nose shapes and initial velocities, the relationship between non-dimensional depth P/L_{eff} and I_{ln}^* of each set of experiments can be arranged into linear relations, where in each line only the initial velocities differ and amongst lines only the nose geometries differ, supporting the afore assumption that the comprehensive I_{ln}^* can be approximately taken as the influence of nose geometry for ogival nose projectiles. The lower ones, representing strictly geometrically scaled data where N_1' is strictly the same [14] due to the same projectile nose shape of $\psi = 1.5$ and shank configuration, are almost arranged exactly along a straight line, even though the sizes of projectiles involved are different as high as up to 10 times in diameter and 1000 times in mass. The ones just beside the data of $\psi = 1.5$, depicted by diamond and star markers, sharing the same nose shape where $\psi = 2$, are also arranged in a line [12, 16]. The middle line sets of $\psi = 3$ show the same trend but scattered due to the difference of the corresponding Y. However, for the same set experiments that the projectile and target properties are same, they are still arranged into linear relations, meaning that the validity of linear relation still works within the same set of experiments. The upper ones are experiments of $\psi = 4.25$, which are also arranged into linear relations.

According to Eq. (11), the gradient in Fig. 4 stands for $D_n^p = \frac{\rho_p v_0^2}{AY}$, which can be derived from D_n^t by the relation of $D_n^p = \frac{\rho_p}{\rho_t}D_n^t$. As shown in Fig. 5 that the relation between $I_{ln}^* = \frac{\ln(1+I^*)}{I^*}$ and $I^* = \frac{N_2}{N_1'}\frac{\rho_t v_0^2}{AY}$ can be approximately taken as linear relations. As a result, the gradient (D_n^p) in Fig. 4 can be derived as $D_n^p = \frac{\rho_p}{\rho_t}I_{ln}^*N_1'/N_2$ where N_1' can be taken as a constant [11], especially for the same or scaled geometry. In

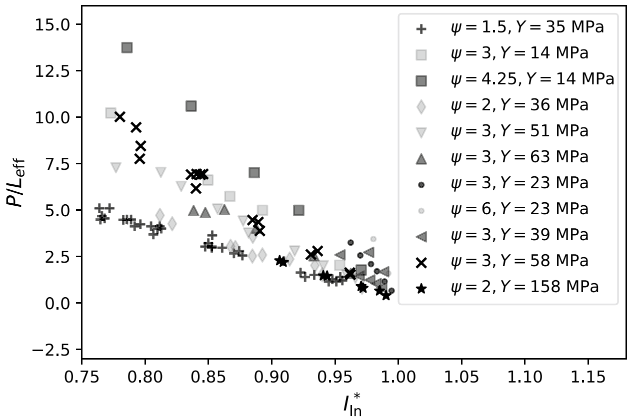

Fig. 4 Relationship between P/L_{eff} and I^*_{ln} [1, 2, 12, 14–16]

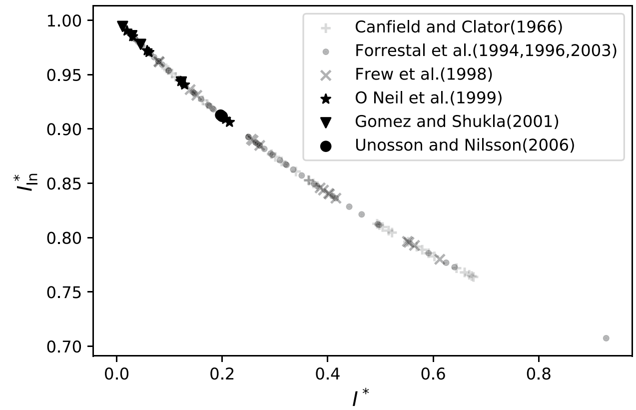

Fig. 5 Relationship between I^*_{ln} and I^* within concerned velocities and projectile shapes [1, 2, 12, 14–18]

other words, the gradient in Fig. 4 approximately satisfies $D^p_n \approx I^*_{ln}/N_2$ when the target and projectile materials are identical and projectile geometries are identical or scaled. Hence, as shown in Fig. 4, at the same value of I^*_{ln}, the gradient increases with the increase of projectile CRH ψ or with the decrease of N_2, or the sharper the penetrator is (i.e., ψ is larger), the deeper the normalized penetration P/L_{eff} would be for the same value of I^*_{ln}.

As shown in Eq. (13) and Fig. 5, I^*_{ln} is a natural logarithm function of I^* and decreases monotonically with the increase of I^*. In order to get a deeper penetration depth, a smaller value of I^* is preferred. As discussed afore, for the same target properties and projectile initial velocities, penetration depth can be increased by decreasing the value of N_2 in I^*, i.e., to make the nose sharper. However, with the increase of projectile nose sharpness, the nose becomes easier to fail under high impact stress. As a result, the design of projectile nose geometry needs to be balanced between its sharpness and resistance to impact loading. For mostly concerned impact velocities ($v_0 < 1200$ m s^{-1}) and projectile nose shapes ($0.5 < \psi < 6$), I^* only ranges from 0 to 1, leading to the corresponding I^*_{ln} varying from 1 to 0.75, as shown in Fig. 5. If the median 0.85 is taken to approximate I^*_{ln} as a constant, representing the range of I^*_{ln} between 0.75 and 0.95 corresponding to initial impact velocity of approximately 200 to 1200 m s^{-1}, the maximum uncertainty is less than 13.3% (i.e., $0.10/0.75 \times 100\%$), which is in the range of engineering experimental uncertainty and is acceptable for engineering prediction. Hence, the improvement of optimization about ogival nose projectiles to the most is less than 13.3%, which means the optimization effect on the projectile geometry with ogival nose is approaching its ceiling. Though the uncertainty caused by such simplification is acceptable in engineering prediction, the effect of I^*_{ln} cannot be ignored when a more accurate prediction is demanded, as shown in the comparison between Figs. 2 and 3.

2.3 Coefficient related to friction, N'_1

N'_1 is the coefficient related to friction, it equals to unity when friction is ignored. However, as argued in Ref. [11], friction on the shank cannot be ignored for deep penetration, because the overall friction resistance accounts for around 10% in total penetration resistance. It is shown in Fig. 6 that for small non-dimensional depth P/d (for projectiles in Fig. 6, it is less than 7.5), the data fit well with $P/d = 2I_0/\pi$, where the friction can be neglected because of the minor contribution of friction due to the small penetration depth. However, when P/d is greater than 7.5, the data fit well with $P/d = I_0/2$ where the friction must be considered due to the contribution of friction over a relatively deep penetration depth. In fact, the shifting of good-fitting with experimental penetration depth from $P/d = 2I_0/\pi$ to $P/d = I_0/2$ is attributed to the consideration of both friction and I^*_{ln} [11]. Generally, small penetration depth is associated with low initial velocity and large I^*_{ln} (almost equaling to unity, as shown in Eqs. (9) and (13)) where the effects of friction and I^*_{ln} are negligible, shown as the data fitted well with $P/d = 2I_0/\pi$. In the interested range of projectile nose and velocity range, with the increase of initial impact velocity, P/d increases largely and I^*_{ln} decreases from 1 to 0.75, causing the effects of friction and I^*_{ln} significant and must be considered, shown as the data fitted well with $P/d = I_0/2$. For the detailed discussion of friction on projectile, please refer to Ref. [11].

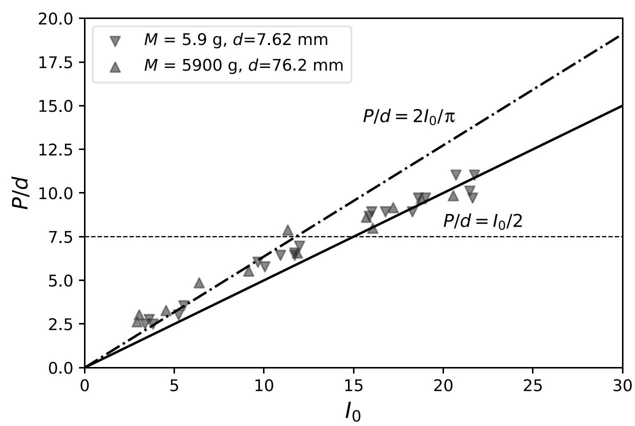

Fig. 6 Relationship between P/d and I_0 for scaled projectiles [12, 14]

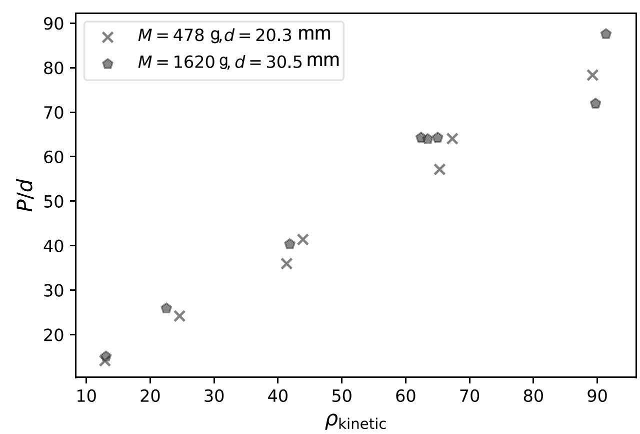

Fig. 7 Relationships between non-dimensional P/d and ρ_{kinetic} for scaled projectiles [2]

3 Applications of penetration similarity to concrete target

3.1 Strictly similar cases

3.1.1 Scaled projectile experiments with high ρ_{kinetic}

Frew et al. [2] carried out penetration experiments into high strength concrete using projectiles with geometrical scaling factor of 2/3. The CRH values for both projectiles are 3. Their masses are 478 g and 1620 g with shank diameter of 20.3 mm and 30.5 mm (i.e., the corresponding mass scaling is 8/27), respectively. The target density and compressive strength are 2320 kg/m^3 and 58.4 MPa. The initial impact velocities vary from 442 to 1225 m s^{-1}.

Figure 7 clearly shows that the relationship between P/d and ρ_{kinetic} meets a linear relationship, though certain deviations happen when ρ_{kinetic} (or v_0) is high due to projectile nose erosion. This relationship can be attributed to that even though the scaled projectiles were quite different in size, but N_1' and I_{ln}^* would be identical in values because of their resemblance (i.e., the same ψ, non-dimensional effective length L_{eff}, D_n^p, and D_n^t), hence, according to Eq. (11), the non-dimensional penetration depth P/d would be left as a linear function of ρ_{kinetic}. The cases shown in Fig. 7 demonstrate the validity of Eq. (11) as the scaling relationship for deep penetration of hard projectiles into concrete targets.

3.1.2 Scaled projectile experiments with low ρ_{kinetic}

Canfield and Clator [14] presented penetration depth data of full-sized and one-tenth scaled steel projectiles into reinforced concrete targets. The CRH values of projectiles are 1.5, and projectile masses are 5.9 g and 5900 g with shank diameters of 7.62 mm and 76.2 mm, respectively. The associated target densities and compressive strengths are 2240 kg/m^3, 34.6 MPa and 2310 kg/m^3, 35.1 MPa, respectively. The prototype projectile is a shell launched from a 76.2 mm naval gun, and the model projectile is a bullet fired from a 7.62 mm caliber rifle. The concrete targets were made with full-size and scaled reinforcing bars and maximum aggregates according to one-tenth scaling factor correspondingly with projectile dimensions.

The results and experiment parameters are listed in Table 1. These data are extracted carefully from Ref. [14].

Figure 8 shows that the relationship between P/d and ρ_{kinetic} of full-sized and one-tenth scaled experiments meets the scaling law very well (i.e., almost a linear relationship), even though they had remarkable one-order magnitude difference in geometrical dimensions and three-order magnitude difference in mass. It is interesting to point out that the same data, which intermittently fitted well with $P/d = 2I_0/\pi$ and $P/d = I_0/2$ in Fig. 6, has unified into a continuous relation of ρ_{kinetic} in Fig. 8. This means that the effects of varying I_{ln}^* and friction resistance for shallow penetration, shown as two discontinuous lines in Fig. 6, can be reflected by the relationship between P/d and ρ_{kinetic} when geometrical scaling conditions are satisfied. The only problem is that, comparing with the excellent linear relationship in Fig. 7, there are some deviations in Fig. 8, especially for small values of ρ_{kinetic}. This is caused by the cratering stage of stochastic scattering or random distributed aggregate, where a particular aggregate with the same size accounts more for small KE projectiles (i.e., low ρ_{kinetic}) than those of high ρ_{kinetic}.

The cases shown in Fig. 8 demonstrate the validity of Eq. (11) as the scaling relationship for shallow penetration of hard projectiles into concrete targets. This means that with the application of ρ_{kinetic}, the penetration depth of proto-type projectile can be reflected by scaled projectiles for both deep (shown in Fig. 7) and shallow (shown in Fig. 8) penetration conditions.

Table 1 Penetration experimental results of scaled projectiles with diameters of 7.62 mm and 76.2 mm

	Diameter 7.62											Diameter 76.2					
v_0 (m s^{-1})	327	338	348	408	419	554	565	589	610	610	617	306	312	381	452	541	602
P (mm)	19	21	19	23	27	46	44	49	49	50	53	200	230	249	370	421	600
P/d	2.5	2.8	2.5	3.0	3.5	6.0	5.8	6.4	6.4	6.6	7.0	2.6	3.0	3.3	4.9	5.5	7.9
v_0 (m s^{-1})	710	713	730	762	769	777	811	826	829	831		616	709	717	742	775	811
P (mm)	66	68	68	68	74	74	84	77	74	84		500	656	608	698	738	750
P/d	8.7	8.9	8.9	8.9	9.7	9.7	11.0	10.1	9.7	11.0		6.6	8.6	8.0	9.2	9.7	9.8

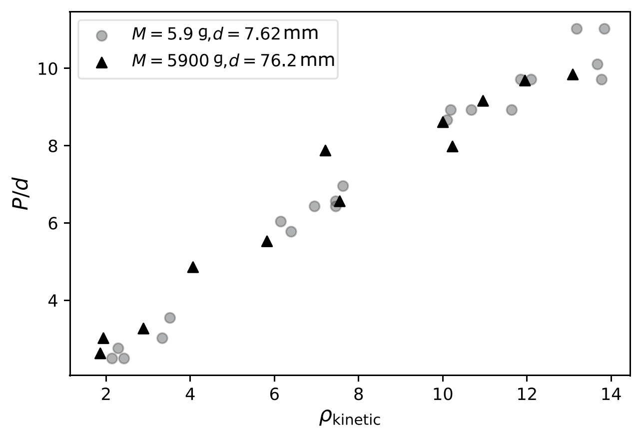

Fig. 8 Relationship between non-dimensional P/d and ρ_{kinetic} for prototype and scaled projectiles with low ρ_{kinetic} [6]

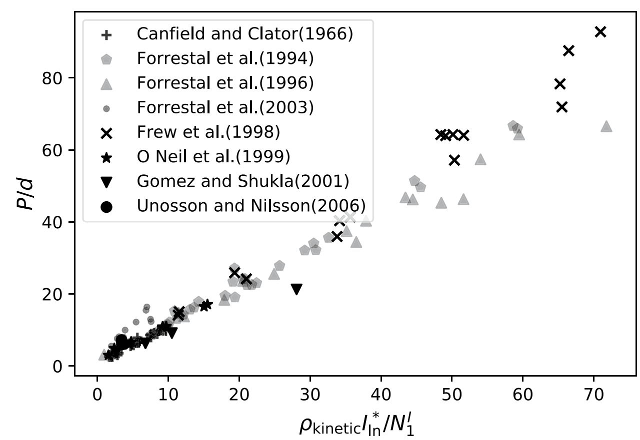

Fig. 9 Relationship between P/d and $\rho_{\mathrm{kinetic}} I_{\mathrm{ln}}^{*}/N_1'$ [1, 2, 12, 14–18]

3.2 Approximately similarity cases

Most of the time, it is hard to meet these strictly ideal similarities, especially for research on some new target materials or projectiles, the practical cases would be more likely to be approximately similar. Benefited from the limited effects of projectile nose and friction [11], these approximate similarity cases still can be approximately unified according to Eq. (11). Figure 9 shows the relationship between P/d and $\rho_{\mathrm{kinetic}} I_{\mathrm{ln}}^{*}/N_1'$. It can be seen that though the projectiles are different remarkably, there is a linear trend depicted in Eq. (11) among them. It fits well with experiments when $\rho_{\mathrm{kinetic}} I_{\mathrm{ln}}^{*}/N_1'$ is low, but deteriorated when it is high. This can attribute to the severe abrasion on the projectile nose, which can account for up to 70% or 46% of the nose mass (though deceptively only 7.0% or 4.6% of the total projectile mass), depending on the corresponding ρ_{kinetic} [1, 2]. It should be noted that Eq. (11) is deduced on the assumption that the projectile is rigid, where the projectile nose geometry keeps the same and penetration capacity of projectiles with different nose geometries can be unified by the definition of I_{ln}^{*}.

4 Conclusions

In this paper, three non-dimensional quantities, i.e., ρ_{kinetic}, I_{ln}^{*} and N_1' are proposed to provide a better understanding of the similarity and scaling law in rigid-body penetration depth. The effects and physical meanings of each of them are discussed based on the comparisons between experimental data and general resistance formulas considering friction. The similarities in penetration depth, from small to large, of rigid ogival nose projectiles are discussed based on the similarity quantities and relationships.

More specific conclusions are as follows:

1. Similarity relations in penetration depth of concrete with rigid body can be demonstrated by the multiplication of three non-dimensional quantities: ρ_{kinetic}, the non-dimensional areal density of projectile KE relative to non-inertia resistant stress of target at the interactive cross section between projectile and target; I_{ln}^{*}, combined factor of projectile nose geometry and $D_{\mathrm{n}}^{\mathrm{t}} = \frac{\rho_t v_0^2}{AY}$; and N_1', coefficient related to the friction. For identical

or scaled projectile geometry, N_1' would be the same, and if identical target and projectile materials and initial impact velocity are added, $I_{\ln}^*$ would be left as the only function of projectile nose geometry (N_2).

2. The penetration capacities of ogival nose projectiles are dominated by ρ_{kinetic}, which is consisted by non-dimensional quantity $D_{\text{n}}^{\text{p}} = \rho_{\text{p}} v_0^2/(AY)$ with the same form as Johnson's damage number and non-dimensional effective length L_{eff}/d. After excluding the influences of projectile nose geometry and friction, it can be concluded that P/d is directly linearly controlled by D_{n}^{p}, enhanced by L_{eff}/d under the multiplication relation, and optimized by projectile nose geometry in the formation of $I_{\ln}^*$.
3. The non-dimensional penetration depths of ogival nose projectiles can be unified with each other according to Eq. (11). For strictly scaled projectiles, this relationship for shallow and deep penetration can be simplified into the same function in terms of ρ_{kinetic}.
4. The projectile nose effect and the term $\bar{Y}$ in Johnson's damage number can be accounted by mutual effect factor of nose geometry $I_{\ln}^*$ and concrete dynamic strength resistance AY in penetration, respectively.

Acknowledgments The first author would like to acknowledge the scholarship granted by the China Scholarship Council and the support from the Institute of Chemical Materials, CAEP. The authors greatly appreciate financial support from the National Natural Science Foundation of China (Grants 11702266, 11972329, 51703211, and 11902301).

References

1. Forrestal, M.J., Frew, D.J., Hanchak, S.J., et al.: Penetration of grout and concrete targets with ogive-nose steel projectiles. Int. J. Impact Eng. **18**(5), 465–476 (1996)
2. Frew, D.J., Hanchak, S.J., Green, M.L., et al.: Penetration of concrete targets with ogive-nose steel rods. Int. J. Impact Eng. **21**(6), 489–497 (1998)
3. Chen, X.W., Li, Q.M.: Deep penetration of a non-deformable projectile with different geometrical characteristics. Int. J. Impact Eng. **27**(6), 619–637 (2002)
4. Meng, F.L., Ma, T.B., Xu, X.Z.: Experimental and theoretical investigation of the failure behavior of a reinforced concrete target under high-energy penetration. Acta. Mech. Sin. **36**(1), 116–129 (2020)
5. He, T., Wen, H.M., Guo, X.J.: A spherical cavity expansion model for penetration of ogival-nosed projectiles into concrete targets with shear-dilatancy. Acta. Mech. Sin. **27**(6), 1001–1012 (2011)
6. Peng, Y., Wu, H., Fang, Q., et al.: Geometrical scaling effect for penetration depth of hard projectiles into concrete targets. Int. J. Impact Eng. **120**, 46–59 (2018)
7. Wu, H., Li, Y.C., Fang, Q., et al.: Scaling effect of rigid projectile penetration into concrete target: 3D mesoscopic analyses. Constr. Build. Mater. **208**, 506–524 (2019)
8. Peng, Y., Wu, H., Fang, Q., et al.: Modified spherical cavity-expansion model for projectile penetration into concrete targets. Acta Mech. Sin. **35**, 518–534 (2019)
9. Zhang, J., Chen, W.S., Hao, H., et al.: Performance of concrete targets mixed with coarse aggregates against rigid projectile impact. Int. J. Impact Eng. **141**, 103565 (2020)
10. Deng, Y.J., Song, W.J., Chen, X.W., et al.: Spherical cavity-expansion model for penetration of reinforced-concrete targets. Acta Mech. Sin. **35**, 535−551 (2019).
11. Chai, C.G., Pi, A.G., Li, Q.M., et al.: On the friction effects in rigid-body penetration of concrete and aluminium-alloy targets. Def. Technol. **15**, 576–581 (2019)
12. Forrestal, M.J., Altman, B.S., Cargile, J.D., et al.: An empirical equation for penetration depth of ogive-nose projectiles into concrete targets. Int. J. Impact Eng **15**(4), 395–405 (1994)
13. Rosenberg, Z., Dekel, E.: The deep penetration of concrete targets by rigid rods – revisited. Int. J. Protect. Struct. **1**(1), 125–144 (2010)
14. Canfield, J.A., Clator, I.: Development of a scaling law and techniques to investigate penetration in concrete. Tech. Rep. NWL (Report No. 2057), U.S. Naval Weapons Laboatory, Dahlgren, VA (1966)
15. Forrestal, M.J., Frew, D.J., Hickerson, J.P., et al.: Penetration of concrete targets with deceleration-time measurements. Int. J. Impact Eng. **28**(5), 479–497 (2003)
16. O'Neil, E.F., Neeley, B.D., Cargile, J.D.: Tensile properties of very-high-strength concrete for penetration-resistant structures. Shock Vibr. **6**(5), 237–245 (1999)
17. Gomez, J.T., Shukla, A.: Multiple impact penetration of semi-infinite concrete. Int. J. Impact Eng. **25**(10), 965–979 (2001)
18. Unosson, M., Nilsson, L.: Projectile penetration and perforation of high performance concrete: experimental results and macroscopic modelling. Int. J. Impact Eng. **32**(7), 1068–1085 (2006)
19. Kong, X.Z., Wu, H., Fang, Q., et al.: Projectile penetration into mortar targets with a broad range of striking velocities: test and analyses. Int. J. Impact Eng. **106**, 18–29 (2017)
20. Johnson, W.: Impact Strength of Materials. Edward Arnold, London (1972)